

3D-Aware Scene Manipulation via Inverse Graphics

Shunyu Yao *
 Tsinghua University
 shunyuyao.cs@gmail.com

Tzu Ming Harry Hsu *
 MIT CSAIL
 stmharry@mit.edu

Jun-Yan Zhu
 MIT CSAIL
 junyanz@mit.edu

Jiajun Wu
 MIT CSAIL
 jiajunwu.cs@gmail.com

Antonio Torralba
 MIT CSAIL
 torralba@mit.edu

Bill Freeman
 MIT CSAIL, Google Research
 billf@mit.edu

Joshua Tenenbaum
 MIT CSAIL
 jbt@mit.edu

Abstract

We aim to obtain an interpretable, expressive and disentangled scene representation that contains comprehensive structural and textural information for each object. Previous representations learned by neural networks are often uninterpretable, limited to a single object, or lack 3D knowledge. In this work, we address the above issues by integrating 3D modeling into a deep generative model. We adopt a differentiable shape renderer to decode geometrical object attributes into a shape, and a neural generator to decode learned latent codes to texture. The encoder is therefore forced to perform an inverse graphics task and transform a scene image into a structured representation with 3D attributes of objects and learned texture latent codes. The representation supports reconstruction and a variety of 3D-aware scene manipulation applications. The disentanglement of structure and texture in our representation allows us to rotate and move objects freely while maintaining consistent texture, as well as changing the object appearance without affecting their structures. We systematically evaluate our representation and demonstrate that our editing scheme is superior to 2D counterparts.

1 Introduction

Humans are incredible at perceiving the world, but more distinguishing is the ability to simulate and imagine what will happen within our mind. Given a photo taken on the road as in Fig. 1, we can not only effortlessly detect and recognize cars, understand their physical dynamics with our prior knowledge, encode visual appearances as learned concepts, but more interestingly, based on these pieces of information, imagine how cars might move and rotate in the 3D world. Motivated by such human abilities, in this work we seek to obtain an interpretable, expressive, and disentangled scene representation for machines, and employ the learned representation for flexible scene manipulation.

Nowadays, deep generative models [Goodfellow et al., 2014, Kingma and Welling, 2014, van den Oord et al., 2016] have led to remarkable breakthroughs in learning hierarchical representations of images and decoding the representation back to images. However, the obtained representation is often limited to a single isolated object and is rarely interpretable or able to take into account the complex 3D structure underlying the image. As a result, these deep generative models cannot support simulation tasks such as moving an object around in Fig. 1. On the other hand, graphics engines use

* denotes equal contribution

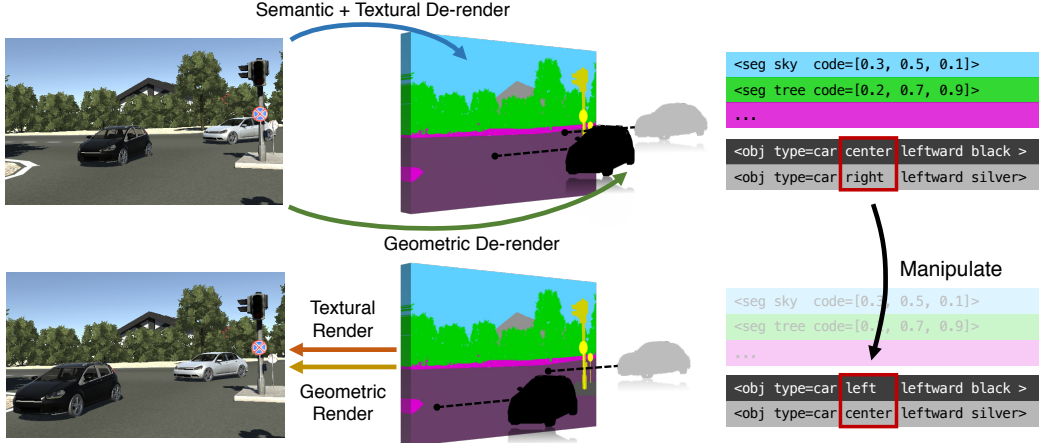


Figure 1: We propose to learn a holistic scene representation that encodes scene semantics and instance-wise information like texture and 3D attributes. Via our generative model, the learned representation supports image reconstruction and allows a user to edit the appearance and 3D properties of individual objects.

a predefined structured and disentangled input (i.e. graphics code) to render images and can easily manipulate scenes. However, it is in general intractable to recover the graphics code from the image. The existing 3D rendering process is often non-differentiable.

In this paper, we take advantage of both model-based and learning-based methods to obtain an interpretable and structured scene representation. In one branch dealing with 3D geometric structure, we detect objects, infer their structural attributes, and learn through an approximately differentiable renderer. In the other branch dealing with color and texture, we adopt a semantic encoder to obtain the instance label map of an image, and jointly train an object-wise texture encoder and a texture generator to decode the texture latent codes back to the pixels. The 3D attribute inference network and the instance texture encoder are enforced to perform inverse graphics tasks of the shape renderer and the texture generator via the image reconstruction loss. By disentangling 3D structure from texture in both the recognition and the generative model, we can more readily perform manipulation tasks. For example, to move a car closer, we can simply edit its 3D attributes such as position and pose, but leave the texture and semantics unchanged. The texture generator is also able to synthesize diverse texture on the same shape.

We report quantitative and qualitative results to demonstrate the effectiveness of our framework on two datasets, Virtual KITTI [Gaidon et al., 2016] and Cityscapes [Cordts et al., 2016]. Since the 3D-aware scene manipulation problem has not been well formulated, besides providing a variety of manipulation examples, we create an image editing benchmark on Virtual KITTI to evaluate our model against 2D pipelines capable of doing so. We also investigate the design of our model through evaluations on representation accuracy and image reconstruction quality. Our user-friendly editing system and our models will be available upon publication.

2 Related Work

Interpretable image representation Our work is closely related to a line of work in obtaining interpretable image representations with neural networks. DC-IGN [Kulkarni et al., 2015] achieved this by freezing a subset of latent codes while feeding images that move along a certain direction in the image manifold. A recurrent model [Yang et al., 2015] was developed to alter latent factors. Chen et al. [2016] proposed to automatically disentangle an image into independent factors without supervised data. While all these work focused on imagery of a single visual object, we aim to understand our natural scene in a holistic way. Our work most resembles Wu et al. [2017] as it studied the problem on a general scene image, with a graphics engine as the decoder and a neural network as encoder to perform the inverse graphics task. However, it is infeasible to back-propagate the gradients from the graphics engine or generalize to a new environment, and the results were limited to simple gaming environment such as Minecraft. Different from Wu et al. [2017], we use neural networks as our differentiable encoder and decoder, making it possible to handle complex visual world.

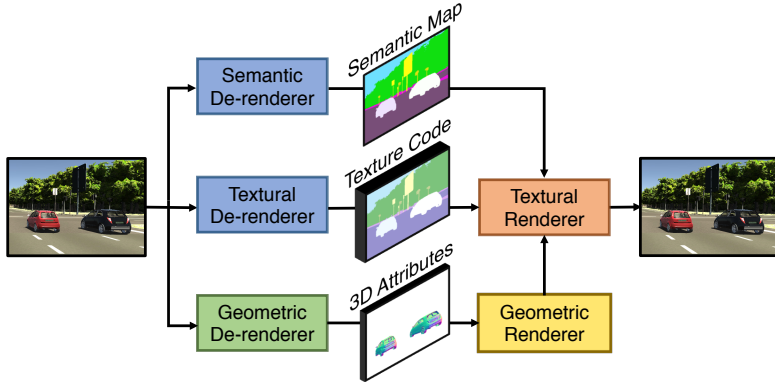


Figure 2: **Illustration of our framework.** The encoder consists of a semantic-, a textural- and a geometric de-renderer, the output representations of which would be combined in a texture renderer to reconstruct the input image.

Deep generative models Deep generative models such as Variational Autoencoders [Kingma and Welling, 2013] and Generative Adversarial Networks [Goodfellow et al., 2014] have been used to synthesize and reconstruct images and learn rich internal representations of images. Unfortunately, the learned representation is often difficult for humans to interpret. Besides, existing deep generative models fail to take into account the complex 3D nature of the world. On the contrary, our differentiable shape renderer can discover the 3D geometric structure of objects, which improves the image reconstruction quality and also paves the way for 3D-aware scene manipulation.

Deep image manipulation Recently, neural networks have supported various image processing tasks, such as photo enhancement [Yan et al., 2015], style transfer [Gatys et al., 2016, Selim et al., 2016], inpainting [Pathak et al., 2016], denoising [Gharbi et al., 2016] and so on. Nevertheless, previous methods concentrate on a 2D setting. One of our main contributions is to introduce 3D awareness into the realm of deep image manipulation. On top of that, traditional image manipulation methods often require a certain structured representation as input such as label maps, while our framework can learn a proper representation by itself and allow users to perform white-box modifications on input images.

3 Method

Here we present our solution to scene de-rendering problem and its applications. We begin with an overview of our framework and our representation, and then describe the model and its implementation in details.

3.1 Overview

Encoder-Decoder Framework In our encoder-decoder framework, we first de-render(encode) an image into a compact representation. Then a renderer (decoder) reconstructs the image from the representation. Figure 2 illustrates three branches for extracting semantic, 3D geometric and textural information from the image, respectively. The semantic branch aims to produce an instance label map of the image. The texture branch learns to encode the color and texture of each object instance into a latent texture code so that the texture can be reconstructed from the code later. The 3D geometric branch infers 3D attributes of objects and adopt a differentiable shape renderer to decode the 3D attributes to shapes.

A Disentangled Representation An image can be decomposed into a background and a number of foreground objects. Each segment in the background or object in the foreground has a unique instance ID. While for each instance the texture branch learns a latent texture code that supports texture reconstruction, in the 3D geometric branch we only deal with objects of interest. We formulate the geometric structure of each object by a mesh model with predefined 3D attributes. Thus for each object, we encode its 3D attributes and a texture latent code for representation, with two parts treated in separate branches.

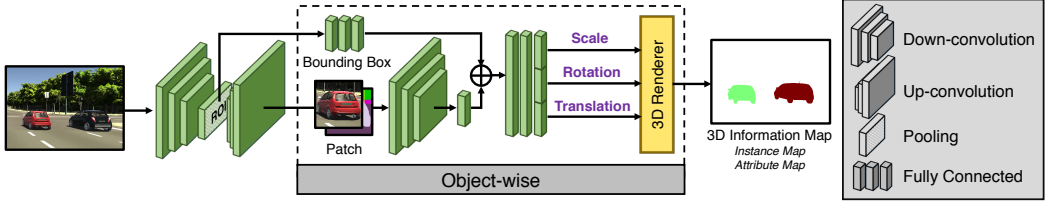


Figure 3: **The geometric interpretation module.** The module takes the whole image, infers 3D attributes with proper formulations from object proposals, and can generate interpretable representations for understanding and manipulation.

3.2 3D Geometrical Inference

One of our feature stems from a design of 3D geometrical understanding framework as shown in Figure 3. To handle the geometry of objects in a scene, first we generate proposals of image patches and their silhouettes based on its objectness. For each proposal, we aim to describe the object with an intrinsic mesh model M and a extrinsic pose π related to the observer. Furthermore, we enforce its re-projection onto 2D image to be consistent with the observation.

3D Attributes We characterize an object by a mesh model $M = (V, F)$ of vertices and faces, along with additional attributes π : scale $s \in \mathbb{R}^3$, rotation represented by an unit quaternion $q \in \mathbb{R}^4$, and translation $t \in \mathbb{R}^3$. This characterization can fully determine an object’s 3D configuration. However, for most real-world scenarios, especially road scenes, we assume that for all objects their bottom face lies parallel to the ground, i.e. the quaternion possesses only a rotational degree of freedom $q = q(\theta)$.

For most applications which aim to recover geometric configurations, they are limited to one or a few objects that lies within a confined range, and however when we address multiple objects in a scene, we argue that to result in the same perceptual difference, which is angular, we require a certain percentage change in translation, namely $|\delta t|/|t| = \delta \log |t|$. When it is more feasible to make inference in the log-space in distances, the patch on its own cannot give distance description, since the distance conditioned on the patch is not a well-distributed quantity as illustrated in the left part of Figure 4a. We propose to fix this problem by reparametrizing the translation by $t = \|t\|_2 \hat{e} = \frac{\tau}{\sqrt{A}}(\hat{e}_0 + \Delta e)$, where \hat{e}_0 is a unit translation towards the center of the bounding box, A is the area of the bounding box. Out of the two variables of interest, $\tau \in \mathbb{R}$ is the normalized distance, and $\Delta e \in \mathbb{R}^3$ alters the direction. Figure 4a exhibits that the proposed distance τ has a more concentrated distribution and hence possibly a smaller inference error. Let $\tilde{\cdot}$ denote inferred attributes as (\cdot) being the ground truth symbol, we define the loss on π as

$$\mathcal{L}_\pi = \sin^2 \left(\frac{\theta - \tilde{\theta}}{2} \right) + \lambda_1 \|\Delta e - \Delta \tilde{e}\|_2^2 + \lambda_2 (\log \tau - \log \tilde{\tau})^2 + \lambda_3 \|s - \tilde{s}\|_2^2. \quad (1)$$

Re-projection Consistency Solely fitting the structural attributes does not guarantee that the model can fit our perception. Therefore, we propose to enforce constraints on the recovered image from the inferred 3D representations as shown in Figure 4b. The task is not usually straightforward as standard graphics engine are often not differentiable and the errors in appearance matching cannot back-propagate to the de-renderer as in classical neural network training paradigms. To address this issue, Loper and Black [2014], Kato et al. [2018] compute, on top of a mesh representation, approximate gradients for neural network training. By adopting approximately differentiable renderers, we can render 3D-aware maps for the scene such as instance-label maps \tilde{L} , with which we define the re-projection loss as

$$\mathcal{L}_M = \|\mathbf{L} - \tilde{\mathbf{L}}\|_1. \quad (2)$$

3.3 Semantic and Texture Inference

Inspired by recent image-to-image translation methods [Isola et al., 2017, Wang et al., 2018], we analyze the 2D information of a scene similar to their setup. Two separate convolutional networks are employed to obtain necessary color and texture description codes for either a segment in the background (e.g. road, sky) or an object in the foreground (e.g. car, van). Specifically, a semantic

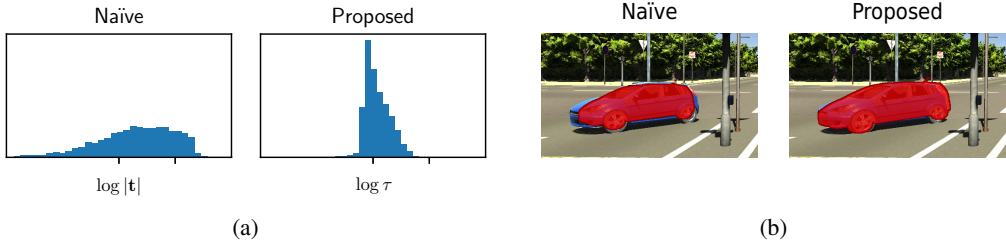


Figure 4: **Proposed improvements to the de-rendering task.** (a) Distributions of the original distance $|t|$ compared to proposed normalized distance τ . x axes are of equal stretches. (b) Object silhouettes rendered without and with our proposed re-projection loss.

segmentation network and a detection-based instance proposal network are combined to obtain an instance label map \mathbf{L} .

An object instance often appears with independent but coherent visual appearance. Hence the texture network is designed to build a correspondence between the appearance of an instance and a latent code that represents it. Formally speaking, Given an image \mathbf{I} and its instance label map \mathbf{L} , we want to obtain an instance-wise feature map \mathbf{z} such that (\mathbf{L}, \mathbf{z}) can be used to reconstruct \mathbf{I} . We pose the problem in a conditional generative modeling setting as a tuple (G, D, E) : a texture encoder $E : (\mathbf{L}, \mathbf{I}) \rightarrow \mathbf{z}$, a generator $G : (\mathbf{L}, \mathbf{z}) \rightarrow \mathbf{I}$ and a discriminator $D : (\mathbf{L}, \mathbf{I}) \rightarrow (0, 1)$ are trained jointly for this purpose.

Three objectives are considered for different purposes. First, a standard GAN loss is used as

$$\mathcal{L}_{\text{GAN}}(G, D, E) = \mathbb{E}_{\mathbf{L}, \mathbf{I}}[\log(D(\mathbf{L}, \mathbf{I})) + \log(1 - D(\mathbf{L}, G(\mathbf{L}, E(\mathbf{L}, \mathbf{I}))))]. \quad (3)$$

The second term is an L1 loss imposed on features in the intermediate layers and thus the output image is perceptually close to a real image:

$$\mathcal{L}_{\text{Per}}(G, E) = \mathbb{E}_{\mathbf{L}, \mathbf{I}} \left[\frac{1}{n} \sum_{i=1}^n \|F_i(\mathbf{I}) - F_i(G(\mathbf{L}, E(\mathbf{L}, \mathbf{I})))\|_1 \right]. \quad (4)$$

Here F_i denotes the feature extractor at layer i of a convolutional network. The last term is an L1 loss on image reconstruction:

$$\mathcal{L}_{\text{Recon}}(G, E) = \mathbb{E}_{\mathbf{L}, \mathbf{I}}[\|\mathbf{I} - G(\mathbf{L}, E(\mathbf{L}, \mathbf{I}))\|_1]. \quad (5)$$

Put together, the texture network is formulated as a minimax game between (G, E) and D described below.

$$G^*, E^* = \arg \min_{G, E} \max_D (\mathcal{L}_{\text{GAN}}(G, D, E) + \gamma_1 \mathcal{L}_{\text{Per}}(G, E) + \gamma_2 \mathcal{L}_{\text{Recon}}(G, E)). \quad (6)$$

3.4 Leveraging 3D Geometric Knowledge for Better Texture

Separating information into geometric and textural branches in the model does not necessarily decouple geometric information from the textural information. When the textural branch does not receive geometric cues, we observe the textural encoder tends to learn jointly the object texture pattern and its specific pose instead of only the texture. We provide an easy yet effective fix by concatenating object pose attributes attained by the geometric branch, to the texture code map \mathbf{z} , and feed it as the new input to the texture generator G . Also, we lower the texture feature code dimension to discourage its coupling with pose. This strategy helps recover texture features independent of geometric factors, and at the same time empowers the texture generator to produce better images by removing object pose ambiguity.

3.5 Implementation Details

Our semantic branch adopts a pretrained semantic segmentation model [Zhou et al., 2017], and a MaskRCNN [He et al., 2017] model for object detection and mask generation. Then, we combine those object masks with semantic segmentation results by resolving any conflict in favor of the object

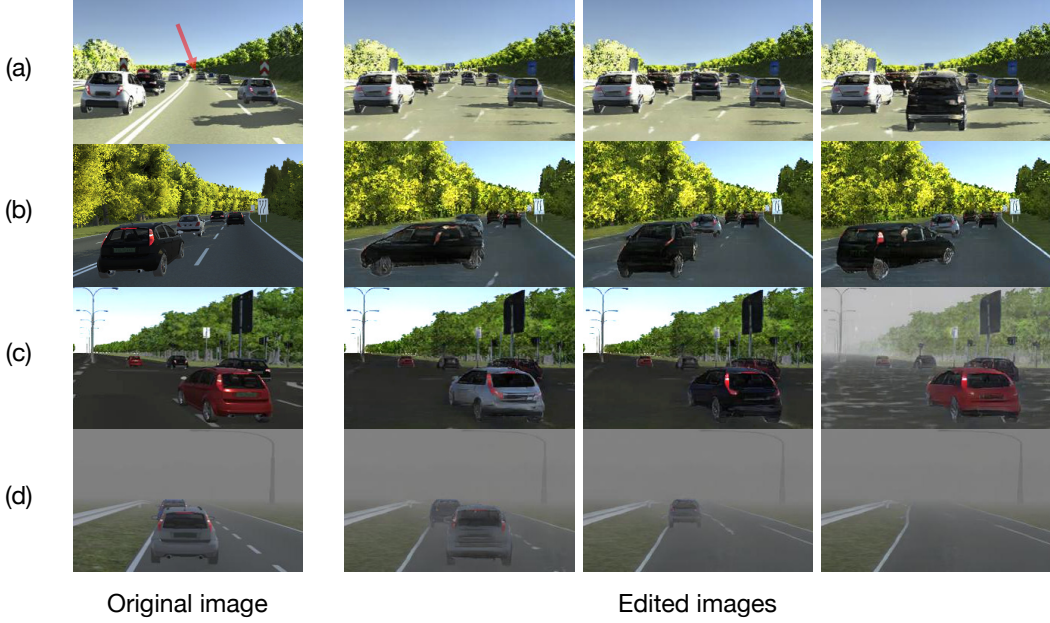


Figure 5: **Image editing examples on Virtual KITTI.** (a) A car far away can be pulled closely with consistent texture. (b) A car can be rotated by only changing its pose code. The same texture code is used for different poses. (c) We use texture codes from cars of different poses on the red car without affecting its pose. We can also change the texture codes of background segments. (d) We show occlusion recovery and object removal schemes.

masks. The instance map is used for the texture branch and the object proposals with masks are fed to the geometric branch.

For our geometric branch, we simplify the problem by picking a general car model from ShapeNet [Chang et al., 2015] and use the mesh model across all cars of interest. Image patches of object proposals are fed through a ResNet-18 [He et al., 2015] network and rendered with Neural 3D Mesh Renderer [Kato et al., 2018]. In \mathcal{L}_π , we empirically set λ 's to 1 for all optimization purposes. We first train with \mathcal{L}_π using Adam [Kingma and Ba, 2015] optimizer and a learning rate of 10^{-3} for 128 epochs, then fine-tune the network with \mathcal{L}_M on a learning rate 10^{-4} for the same amount of epoch.

For our texture branch, we refer to Wang et al. [2018] for the architectures of the encoder, generator, and discriminator. The dimension of texture code is set to 3 on Virtual KITTI and 5 on Cityscapes. The rendered object poses θ are quantized into 24 bins and concatenated to the texture code map \mathbf{z} as a one-hot map. We use hyperparameters $\gamma_1 = 5$, $\gamma_2 = 20$ to train on Virtual KITTI for 60 epochs and Cityscapes for 100 epochs.

4 Results

We report the results in three parts. First, we present new 3D-aware image editing applications enabled by our framework. Second, we build a Virtual KITTI [Geiger et al., 2012] Image Editing Benchmark and compare our editing scheme to baselines without 3D knowledge. Lastly, we analyze our design through evaluating representation accuracy and reconstruction quality.

Data We conduct experiments on two datasets, the first being Virtual KITTI [Gaidon et al., 2016]. The dataset serves as a proxy to the KITTI dataset [Geiger et al., 2012], containing 5 virtual worlds, each rendered under 10 environment conditions (topics), leading to a sum of 21,260 images. Across all our experiments, we partition, according to our Image Editing Benchmark, into a 80%-20% train and test split. The splits are identical across all topics and comprise of consecutive frames only for both train and test split. For object-wise evaluations, we extract objects that are visibly larger than 16×16 square pixels, an occlusion ratio of less than 70%, and a truncation ratio of less than 50% for calculation. The second dataset examined is Cityscapes [Cordts et al., 2016] which ships without ground truth pose annotations and yet is annotated to pixel-level for 2975 training images. We

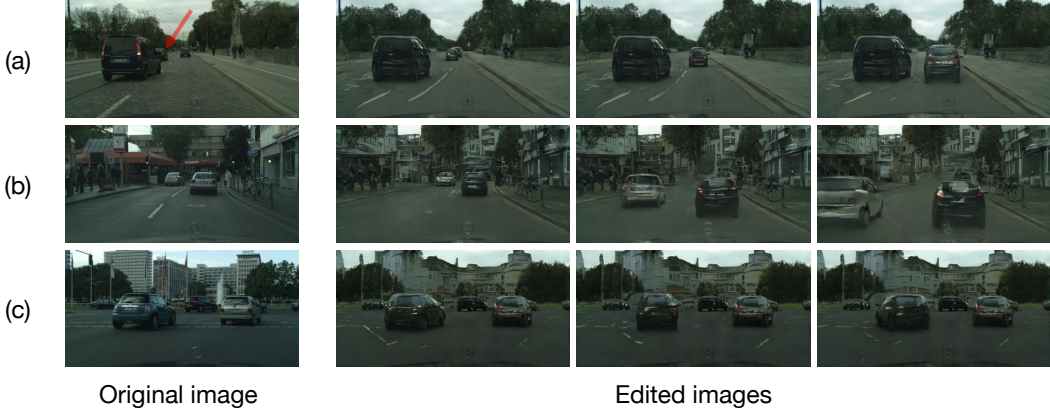


Figure 6: **Image editing examples on Cityscapes.** (a) We recover an occluded car by moving it right then pulling it backward. (b) We design trajectories for two cars to simulate a driving viewpoint. (c) We rotate the left car with small angles.

emphasize only on the category of cars and unless otherwise stated, numbers and visual illustrations are reported over the test set.

4.1 3D-Aware Image Editing

The rich structural and textural information inside our representation brings a built-in image manipulation scheme. Notably, we find the geometric and textural information within our representation to be largely disentangled. We can conduct white-box modifications on the 3D attributes of an object to translate, scale or rotate it in the 3D world while keeping the texture consistent. To change appearances of an object, texture codes from other objects can be adapted without polluting its pose. Please refer to Fig. 5 and Fig. 6 for our manipulations in detail.

As stated before, the Cityscapes dataset does not contain groundtruth object poses for fine-tuning, and hence we exploit the differentiable renderer by first making attribute inferences based on the trained de-renderer, then iteratively optimizing the attributes via re-projection. The resulting geometric attributes turn out to be useful for manipulation tasks.

4.2 Virtual KITTI Image Editing Benchmark

Based on Virtual KITTI, we built a subset of paired images that allows users to evaluate image editing tasks, to which we refer as Image Editing Benchmark. The benchmark contains 92 pairs of images chosen from varying worlds but the same topics with the camera either stationary or almost still. These pairs, an example of which is presented on the left of Figure 1, are only taken from either the first 20% or the last 20% of the frames, which would be taken as test set while the rest shall be treated as the training set. Please refer to the supplementary material for example images.

For each pair of source and target images, we provide an operation for each of the object presented. Namely the starting position $(u_{\text{src}}, v_{\text{src}})$, the ending position $(u_{\text{tgt}}, v_{\text{tgt}})$, which are the projections of the object's 3D center, the zoom-in factors ρ and the difference of rotations Δr_y with respect to the y -axis. Note objects can move out of the image, and thus an operation can be characterized as the 6 numbers above and the type being either modify or delete.

Methods We hereby use our full network, together with two simple implementations for comparison. Specifically,

- 2D: The naïve 2D baseline takes the source and target positions, apply the translation and scale based on the provided operation description.
- 2D+: The 2D+ baseline includes operations in 2D, plus simply rotate Δr_y the planar silhouette along y -axis.

Metrics To evaluate the similarity between the edited source image and the desired target image, we cannot simply evaluate on the pixel level, for two images could appear similar whilst intrinsically having a tiny translation, which dramatically increases the metrics such as L1 or L2 loss. Instead, we adopt Learned Perceptual Image Patch Similarity (LPIPS) metric [Zhang et al., 2018] which is tailored specifically alike to human perceptions, ranging from 0 to 1 with 0 being the most similar.

	Ours	2D	2D+
LPIPS (predicted seg)	0.1742	0.1941	0.1946
LPIPS (gt seg)	0.1708	0.1893	0.1902

(a) Perception similarity scores

	2D	2D+
Ours	67.46%	73.48%

(b) Human study results

Table 1: **Evaluations on Virtual KITTI editing benchmark.** (a) The perceptual similarity is evaluated when either the predicted semantic segmentation or the ground truth segmentation is provided to solely evaluate the manipulation power of the model. Lower score is better. (b) Human subjects compare two method pairs, and the percentage shows how likely they prefer the left method to the top. Our method outperforms pure 2D approaches consistently.

We also conduct a human study, where we present the desired target images and two edited source images from different methods to 120 subjects on Amazon Mechanical Turk, and ask them which looks closer to the target image. We then compute, for a pair of methods, how likely one is preferred by human over the other.

4.3 Evaluation on the Geometric Representation

Methods As described in Section 3.2, we adopt multiple strategies to formulate the inference problem, and we hereby compare our full model (full), which is first trained using \mathcal{L}_π then finetuned using \mathcal{L}_M , with three reduced variants as an ablation study to emphasize the importance of our proposed approaches. We also compare these variants to Mousavian et al. [2017] where they have different formulations to 3D bounding boxes as they impose constraints on 3D boxes whilst breaking rotation into multiple bins for classification. To eliminate the effect of object proposal network, we fix the object proposal as the ground truth bounding box and we can hence separately evaluate the inference model itself. We enumerate the models for comparison.

- Ours (π): only optimizes \mathcal{L}_π ; train from scratch.
- Ours ($\pi + M$): optimizes $\mathcal{L} = \mathcal{L}_\pi + \mathcal{L}_M$; train from scratch.
- Quat: uses a rotation space of $\text{SO}(3)$, characterized by a unit quaternion \mathbf{q} .
- Naïve-d: roll back to the original depth in Figure 4a and regress in log space for the distance.

Metrics To quantify the error in the estimated object parameters, we use a variety of measures on different quantities. For each component, we define an error measure Δ describing the discrepancy between the inferred value and the ground truth. For rotation, we compute the geodesic distance $\Delta_q = \cos^{-1} (2(\mathbf{q} \cdot \tilde{\mathbf{q}})^2 - 1)$; for observation direction \mathbf{e} we use the angle between the ground truth and inferred vectors $\Delta_e = \cos^{-1} (\mathbf{e} \cdot \tilde{\mathbf{e}})$; for distance we have absolute logarithm error $\Delta_t = |\log \|\mathbf{t}\|_2 - \log \|\tilde{\mathbf{t}}\|_2|$, and for scale we adopt standard Euclidean distance $\Delta_s = \|\mathbf{s} - \tilde{\mathbf{s}}\|_2$.

On top of errors of inference on individual objects, we as well compute the fraction of incorrectly rendered instance label maps from inferred object attributes per scene, defined as $\Delta_L = \frac{1}{|L|} \|\mathbf{L} \neq \tilde{\mathbf{L}}\|_1$.

Note that in terms of the instance maps we effectively emphasize closer objects, which we have optimized throughout our formulation. All numbers reported are averaged, either over objects or scenes across the test set.

Results Quantitative results are shown in Table 2. Our full model performs the best in terms of multiple criteria, and specifically the mismatch in instance label map outperforms significantly than other formulations. Each of the proposed components (re-projection consistency, normalized depth, constrained rotation, and fine-tuning) contribute to the performance.

5 Conclusion

In this work, we develop an inverse graphics network combining model-based and learning-based techniques. The representation obtained this way is interpretable and disentangled, with rich 3D structural and textural information for each object. Though the representation is mainly applied for 3D-aware scene manipulation in this work, arguably it is suitable for various other tasks like image reasoning, captioning and analogy-making. One favorable future direction is to extend the work to a video setting, where temporal changes in the representation can be explicitly used for physical scene understanding and potential real-world use cases like autonomous driving.

	Rotation (°)	Direction (°)	Distance ($\times 10^{-2}$)	Scale	Label Map ($\times 10^{-3}$)
Ours (full)	2.16	0.295	3.37	0.464	4.60
Ours (π)	2.44	0.397	3.76	0.372	9.54
Ours ($\pi + M$)	2.33	0.333	3.44	0.442	5.24
Quat	5.22	0.380	4.51	0.405	11.23
Naïve-d	2.68	0.357	4.13	0.413	10.15
Bbox3D	5.18	0.341	4.41	0.391	9.80

Table 2: **Performance of inference on Virtual KITTI using ground truth proposals.** We record the performance of our full model, two variants and three other formulations, on all 3D parameters. Our full model performs the best in terms of most metrics except for the scale, which is a trade-off by optimizing for visual coherence at fine-tuning time, and yet for purposes such as re-rendering for 2D manipulations, our full model is greatly favored due to its low error in instance label map. Refer to the text for detailed metric descriptions.

References

Angel X Chang, Thomas Funkhouser, Leonidas Guibas, Pat Hanrahan, Qixing Huang, Zimo Li, Silvio Savarese, Manolis Savva, Shuran Song, Hao Su, Jianxiong Xiao, Li Yi, and Fisher Yu. Shapenet: An information-rich 3d model repository. *arXiv:1512.03012*, 2015. 6

Xi Chen, Yan Duan, Rein Houthooft, John Schulman, Ilya Sutskever, and Pieter Abbeel. Infogan: Interpretable representation learning by information maximizing generative adversarial nets. In *NIPS*, 2016. 2

Marius Cordts, Mohamed Omran, Sebastian Ramos, Timo Rehfeld, Markus Enzweiler, Rodrigo Benenson, Uwe Franke, Stefan Roth, and Bernt Schiele. The cityscapes dataset for semantic urban scene understanding. In *CVPR*, 2016. 2, 6

A Gaidon, Q Wang, Y Cabon, and E Vig. Virtual worlds as proxy for multi-object tracking analysis. In *CVPR*, 2016. 2, 6

Leon A Gatys, Alexander S Ecker, and Matthias Bethge. Image style transfer using convolutional neural networks. In *Computer Vision and Pattern Recognition (CVPR), 2016 IEEE Conference on*, pages 2414–2423. IEEE, 2016. 3

Andreas Geiger, Philip Lenz, and Raquel Urtasun. Are we ready for autonomous driving? the kitti vision benchmark suite. In *CVPR*, 2012. 6

Michaël Gharbi, Gaurav Chaurasia, Sylvain Paris, and Frédo Durand. Deep joint demosaicking and denoising. *ACM Transactions on Graphics (TOG)*, 35(6):191, 2016. 3

Ian Goodfellow, Jean Pouget-Abadie, Mehdi Mirza, Bing Xu, David Warde-Farley, Sherjil Ozair, Aaron Courville, and Yoshua Bengio. Generative adversarial nets. In *NIPS*, 2014. 1, 3

Kaiming He, Xiangyu Zhang, Shaoqing Ren, and Jian Sun. Deep residual learning for image recognition. In *CVPR*, 2015. 6

Kaiming He, Georgia Gkioxari, Piotr Dollár, and Ross Girshick. Mask r-cnn. In *ICCV*, 2017. 5

Phillip Isola, Jun-Yan Zhu, Tinghui Zhou, and Alexei A Efros. Image-to-image translation with conditional adversarial networks. In *CVPR*, 2017. 4

Hiroharu Kato, Yoshitaka Ushiku, and Tatsuya Harada. Neural 3d mesh renderer. In *CVPR*, 2018. 4, 6

Diederik P. Kingma and Jimmy Ba. Adam: A method for stochastic optimization. In *ICLR*, 2015. 6

Diederik P Kingma and Max Welling. Auto-encoding variational bayes. *arXiv preprint arXiv:1312.6114*, 2013. 3

Diederik P. Kingma and Max Welling. Auto-encoding variational bayes. In *ICLR*, 2014. 1

Tejas D Kulkarni, William F Whitney, Pushmeet Kohli, and Josh Tenenbaum. Deep convolutional inverse graphics network. In *NIPS*, 2015. 2

Matthew M Loper and Michael J Black. OpenDr: An approximate differentiable renderer. In *European Conference on Computer Vision*, pages 154–169. Springer, 2014. 4

Arsalan Mousavian, Dragomir Anguelov, John Flynn, and Jana Košecká. 3d bounding box estimation using deep learning and geometry. In *Computer Vision and Pattern Recognition (CVPR), 2017 IEEE Conference on*, pages 5632–5640. IEEE, 2017. 8

Deepak Pathak, Philipp Krahenbuhl, Jeff Donahue, Trevor Darrell, and Alexei A Efros. Context encoders: Feature learning by inpainting. In *Proceedings of the IEEE Conference on Computer Vision and Pattern Recognition*, pages 2536–2544, 2016. 3

Ahmed Selim, Mohamed Elgharib, and Linda Doyle. Painting style transfer for head portraits using convolutional neural networks. *ACM Transactions on Graphics (ToG)*, 35(4):129, 2016. 3

Aaron van den Oord, Nal Kalchbrenner, Lasse Espeholt, Oriol Vinyals, Alex Graves, et al. Conditional image generation with pixelcnn decoders. In *NIPS*, 2016. 1

Ting-Chun Wang, Ming-Yu Liu, Jun-Yan Zhu, Andrew Tao, Jan Kautz, and Bryan Catanzaro. High-resolution image synthesis and semantic manipulation with conditional gans. In *CVPR*, 2018. 4, 6

Jiajun Wu, Joshua B Tenenbaum, and Pushmeet Kohli. Neural scene de-rendering. In *CVPR*, 2017. 2

Zhicheng Yan, Hao Zhang, Baoyuan Wang, Sylvain Paris, and Yizhou Yu. Automatic photo adjustment using deep neural networks. *ACM Transactions on Graphics*, 2015. 3

Jimei Yang, Scott E Reed, Ming-Hsuan Yang, and Honglak Lee. Weakly-supervised disentangling with recurrent transformations for 3d view synthesis. In *NIPS*, 2015. 2

Richard Zhang, Phillip Isola, Alexei A Efros, Eli Shechtman, and Oliver Wang. The unreasonable effectiveness of deep networks as a perceptual metric. In *CVPR*, 2018. 7

Bolei Zhou, Hang Zhao, Xavier Puig, Sanja Fidler, Adela Barriuso, and Antonio Torralba. Scene parsing through ade20k dataset. In *Proceedings of the IEEE Conference on Computer Vision and Pattern Recognition*, 2017. 5